Journal of The Electrochemical Society

The Electrochemical Society
Advancing solid state & electrochemical science & technology

ACCEPTED MANUSCRIPT

Steel Corrosion in Highly Carbonated Solutions Mitigated Using Biphosphate Ions as Inhibiting Agents

To cite this article before publication: Evelyn Tolosa *et al* 2023 *J. Electrochem. Soc.* in press https://doi.org/10.1149/1945-7111/acbc4e

Steel Corrosion in Highly Carbonated Solutions Mitigated Using Biphosphate Ions as Inhibiting Agents

Journal:	*Journal of The Electrochemical Society*
Manuscript ID	JES-108724.R2
Manuscript Type:	Research Paper
Date Submitted by the Author:	01-Feb-2023
Complete List of Authors:	Tolosa, Evelyn; INTEMA, Electroquímica Aplicada Frontini, María; CONICET Mar del Plata Yohai, Lucia; INTEMA, Electroquímica Aplicada Vazquez, Marcela; CONICET Mar del Plata, Valcarce, Maria; INTEMA, Electroquímica Aplicada
Keywords:	Corrosion, Corrosion Inhibitors, Corrosion protection, Passivity

Steel Corrosion in Highly Carbonated Solutions Mitigated Using Biphosphate Ions as Inhibiting Agents

E. Tolosa, M. A. Frontini, L. Yohai, M. Vázquez, and M. B. Valcarce[z]

Facultad de Ingeniería, Universidad Nacional de Mar del Plata,

INTEMA, 7600 Mar del Plata, Argentina

[z]E-mail: mbvalca@hotmail.com

Abstract

The effect of biphosphate ions as potential inhibiting agents for construction steel is analyzed in heavily carbonated solutions (HCS) simulating concrete where $[HCO_3^-] + [CO_3^{=}]) = 0.315$ mol L^{-1}. Three conditions are analyzed, always keeping pH=9: 1) a highly carbonated pore simulating solution (HCS); 2) HCS contaminated with NaCl 0.1 mol/L; and 3) HCS contaminated with NaCl 0.1 mol/L and incorporating biphosphate ions as inhibiting agent. In this last condition, three inhibitor dosages are tested, where the ratios $[HPO_4^{2-}] / [Cl^-]$ are 0.2, 0.6, and 1. The results are compared to previous studies in solutions containing ten times less carbonate content. Several electrochemical and surface techniques are used to correlate inhibiting efficiency of biphosphate ions to dosage. The incorporation of biphosphate ions as inhibitors improves the resistance against localized corrosion. The passivating film is composed of a mixture of phosphates and oxides, mainly Fe(III) species. The inhibition efficiency is sensible to the content of biphosphate and carbonate ions in solution. The optimal dosage of Na_2HPO_4 is 0.06 mol L^{-1}, where the inhibition efficiency evaluated over 6 weeks is higher than 99%. The benefit of using Na_2HPO_4 in proper concentrations as an efficient corrosion inhibitor is demonstrated for the experimental conditions under study.

Introduction

Reinforced concrete is a structural material of widespread use due to its outstanding durability. Nevertheless, the corrosion of the reinforcement bars (construction steel rebars) is an important concern. Corrosion processes affect the performance of concrete structures, particularly of those located close to the seashore [1-3]. Concrete is an alkaline material showing pH values around 13. In most conditions, this environment enables the formation of a passive layer on the rebars that provides effective protection against deterioration by corrosion. Certain factors, such as acidification by CO_2 permeation through the pores' network, or the presence of chloride ions, compromise the stability of this passive film and increase the risk of corrosion [4]. When construction sites are in marine environments, chloride ions can reach the rebars surface by migration or can be added by using contaminated aggregates. Threshold values to quantify the probability of corrosion for different chloride contents are usually given as chloride/hydroxyl ratios [5-7].

Inhibitors can be added to concrete in a variety of forms, and they are a frequent choice when the risk of corrosion by chlorides o carbonation needs to be considered [8-11]. Many anions have been investigated to inhibit rebars' corrosion. The list includes chromate, nitrite, phosphate, citrate, tungstate, and molybdate ions, among others [12-19].

Phosphate ions are an attractive alternative for economic and environmental reasons: they are cost-effective and present low toxicity. This inorganic inhibitor has been extensively investigated. It has proven to be efficient when used to control localized corrosion of rebars in concrete structures [14, 20-26]. However, the results depend on the conditions where it is tested, namely pH, carbonatation, and absolute and relative chloride and phosphate concentrations, among others. Recently, phosphate ions have also been tested in combination with other inhibiting agents [23, 27, 28]. When mixed with organic molecules, migration through concrete pores could be favored, so that phosphates can not only be incorporated into fresh concrete but also used during reparation procedures by applying it to hardened concrete [29, 30].

The pores of concrete are normally impregnated by moisture and the composition of this environment can be simulated in the laboratory using solutions, as extensively reported in the literature [31-34]. Our group has been investigating the effect and mechanism of inhibition by phosphate and biphosphate ions in simulating solutions and in mortars for many years. The starting point was an investigation in alkaline solutions containing chloride ions ($[Cl^-]$ = 0.1 mol/L and pH=13) [14]. For $[PO_4^{3-}]/[Cl^-]$ = 1, pitting was shown to be inhibited due to the formation of an external layer of ferrous phosphate progressively oxidized to ferric phosphate, together with an inner and protective layer composed mainly of magnetite. A follow-up work involved lower $[PO_4^{3-}]/[Cl^-]$ ratios (0.2 and 0.6) and a higher

concentration of chloride ions ($[Cl^-]$ = 0.5 mol L^{-1}) [21]. The lower dosages of inhibitor aimed at reducing costs and minimizing the impact on the mechanical properties when the inhibitor is used in mortars or concrete. For $[PO_4^{3-}]/[Cl^-]$ = 0.6, pitting was found to be inhibited even after 90 days of immersion, with an inhibition efficiency higher than 98%. Instead, the lowest inhibitor dosage ($[PO_4^{3-}]/[Cl^-]$ = 0.2) was not enough to prevent pitting, at least for the high chloride concentration used in this work. The addition of phosphates was later explored in chloride-contaminated mortars [26], where the inhibition efficiency remained above 95% over an evaluation lasting 540 days. The presence of phosphate ions was thought to promote the formation of a more compact surface layer (mainly magnetite). Also, the deposition of $Ca_3(PO_4)_2$ might block pores and contribute to reduce steel corrosion by retarding the diffusion of detrimental species. Finally, sodium biphosphate was tested as corrosion inhibitor in pH=9 solutions with a low content of carbonate ions, while keeping [inhibitor]/$[Cl^-]$=0.2, 0.6 and 1 [22]. When less carbonate ions are present in solution and if no inhibitor is added, steel is active. Electrochemical impedance spectroscopy and polarization curves showed that the resistance to localized attack improved as the amount of biphosphate ions in solution increased. The surface layer became more protective, probably due to the incorporation of phosphate ions to the film. After a prolonged immersion period, steel remained passive when using the higher inhibitor dosage, where the inhibition efficiency exceeded 99%. Instead, for lower dosages, pitting was detected.

The present work continues the series by analyzing the effectiveness of sodium biphosphate as corrosion inhibitor in solutions containing higher concentrations of carbonate and bicarbonate ions. The pH is kept at 9 to simulate concrete pores heavily carbonated, while also being contaminated with chloride ions. In the literature, different solutions have been reported and used to simulate carbonated concrete. Highly alkaline solutions (pH>12.5), saturated $Ca(OH)_2$ solutions or cement powder aqueous suspensions, were acidified by CO_2 bubbling or $NaHCO_3$ addition. In these solutions, the final ratio and total amounts of carbonate and bicarbonate ions depend on the initial pH, being very variable [11, 33, 35, 36]. The ratio and content of these two ions influence the stability of the passive film on steel, as discussed elsewhere [31, 33, 37-39]. The comparison of two carbonation levels is also significant since bicarbonate ions are known to promote the formation of unstable soluble complexes containing Fe(II) and HCO_3^- [40-43]. The efficiency of nitrite ions as inhibiting agents has already been investigated comparing pore carbonated solutions with high and low levels of carbonate and bicarbonate ions [44, 45]. Alonso and Andrade [37] have also shown a decrease in the bicarbonate concentration facilitates the formation of magnetite. These authors stablish in 0.1 and 0.01 mol L^{-1} the respective concentrations of $NaHCO_3$ and Na_2CO_3 which define the limit between activity and passivity for rebars immersed in pore simulating solutions. Thus, the stability of the protective surface layer that develops on steel

depends on the carbonate content and not only on pH (concrete acidification). This is frequently disregarded in the literature, assuming that just setting the pH at 9, irrespective of the carbonate content, is enough to reproduce carbonated concrete and gives context to the comparison presented in this investigation.

Experimental Design

The electrodes were constructed from carbon steel reinforcement slices (Mn 0.635 wt%, C 0.299 wt%, Si 0.258 wt%, Cu 0.227 wt%, other impurities 0.245 wt%). The slices were provided with an electrical contact and then included in polyvinyl chloride (PVC) cylinders using epoxy resin. The exposed geometrical area of steel was 0.50 cm^2. Using sandpaper, the electrodes were abraded down to grit size 1000. A scheme and photograph of a representative sample are presented in Figure 1.

The electrochemical evaluation was carried out in highly carbonated solutions (HCS) with pH=9. This electrolyte simulated the composition of carbonated concrete and consisted of 0.015 mol L^{-1} Na_2CO_3 and 0.3 mol L^{-1} $NaHCO_3$, so that the total carbonate content ($[CO_3^{=}]$ +$[CO_3H^-]$) resulted in 0.315 mol L^{-1}. These carbonate and bicarbonate ions concentrations are 10 times higher than those used before [21, 22, 44]. As discussed in the introduction, the carbonate content affects the stability and composition of the surface film formed on steel [21, 22, 37, 40-43]. Besides, 0.1 mol L^{-1} NaCl was incorporated to HCS (HCS+Cl) to simulate carbonated concrete contaminated with chloride ions.

Speciation curves show that biphosphate ions are the predominant species in phosphate ions equilibria at pH=9 [24, 46]. To evaluate Na_2HPO_4 as an inhibiting agent (I), chloride-contaminated solutions with three different concentrations of Na_2HPO_4 were analyzed: 0.02, 0.06 and 0.1 mol L^{-1}. These conditions will be referred to as (HCS+I/Cl-0.2, HCS+I/Cl-0.6, HCS+I/Cl-1) respectively, where the ratio $[HPO_4^{2-}]$ /$[Cl^-]$ is 0.2, 0.6, and 1, keeping the pH at 9.

A conventional three-electrode electrochemical cell was used. A Hg/HgO electrode with KOH 0.1 mol L^{-1} (MOE, E= 0.174 V vs. SHE) and a Pt electrode were used as a reference and counter-electrode, respectively. The potential values in this work will be reported taking the MOE as reference. Electrochemical tests were carried out employing a Gamry 600 potentiostat.

To carry out the cyclic voltammograms, the electrolyte was deoxygenated for 10 minutes by nitrogen bubbling. The working electrode was pre-conditioned at -850 mV for 5 min to minimize the presence of surface oxides and to produce a repetitive initial situation. Then, the anodic sweep started at -850

mV up to a specific potential, conveniently chosen to prevent localized attack in each electrolyte. The scan rate was 10 mV s^{-1} and 10 consecutive cycles were performed.

Electrochemical impedance spectra were obtained on unpolarized samples, after keeping the electrodes immersed at open circuit potential (OCP) for 24 h, to allow the development of a natural passive film on the surface. The electrodes were aged and tested in the same solution. The frequency sweep ranged from 20 kHz to 5 mHz, with an amplitude of 10 mV_{rms}. The data were analyzed with Zview®.

Anodic polarization curves were performed to investigate pitting after ageing the steel electrodes in the solution of interest at OCP, for 24 hours, in aerated conditions. The potential sweep started at OCP and continued at a rate of 10 mV s^{-1}. To produce a convenient degree of attack, the scan was reversed after reaching 40 µA cm^{-2}. The pitting potential (E_{pit}) was reported when the current density increased abruptly, in association with pits nucleating on the surface.

Raman spectra were recorded using an Invia Reflex Raman confocal spectrophotometer equipped with a 514 nm laser, using 50 s of exposure, at 100% of intensity and with a 50X objective. Several spectra were taken in different regions of the electrode surface, with a laser exposure of 10 µm in diameter. Before recording each spectrum, the sample was removed from the electrochemical cell and dried in a N_2 atmosphere. The spectra were observed to be reproducible and representative results will be shown.

Each of the tests described above was performed not less than three times (usually more than five) with good reproducibility, and so, representative results will be shown.

Weight loss tests were designed as recommended by ASTM D 2688 Standard Test Methods for Corrosivity of Water in the Absence of Heat Transfer [47]. The rebars were cut into discs, with an exposed geometrical area of 5.67 cm^2. They were then abraded with grade 120 emery paper. To carry out weight loss determinations, three previously weighted coupons were immersed in each solution of interest. The solutions in the containers were maintained aerated and at room temperature. The coupons were withdrawn after 6 weeks, and Raman spectra were recorded. After that, the bulky oxides present in the coupons were stripped by dipping the samples for 10 to 60 s in HCl 1 mol L^{-1} and then neutralized with a saturated Na_2CO_3 solution. Independent tests showed that this procedure did not interfere with the substrate. Finally, the coupons were rinsed with water, dried, and finally weighted.

The composition of surface films grown on carbon steel after immersing the electrodes for 7 days at OCP in each electrolyte of interest was investigated by X-Ray Photoelectron Spectroscopy (XPS). After these 192 h, the samples were rinsed with water and then quickly dried using a stream of N_2. The spectra were obtained using a XPS K-Alpha+ Thermo Fisher Scientific. Survey spectra between 0 and

1100 eV binding energy (B.E.) were recorded with 0.1 eV steps and a bandpass of 50 eV. The total acquisition time was 17.1 s. The diameter of the spot being analyzed was 400 µm. The C1s line of carbon was the taken as reference (284.5 eV BE). XPS bands were analyzed employing free software (XPSPEAK 4.1).

Results

The present investigation centers in comparing three conditions where pH=9 and the carbonate/bicarbonate content is ten times higher than in previous studies: HCS, HCS contaminated with chloride ions and HCS contaminated with chloride but incorporating biphosphate ions as inhibiting agent. In this last condition, three inhibitor dosages are tested.

Interesting differences in the response of carbon steel to these electrolytes can first be appreciated while analyzing the cyclic voltammograms recorded in deaerated electrolytes. Figure 2 shows ten cycles of voltammograms of steel in contact with (a) HCS and b) HCS+I/Cl-1, and the results are compared with the tenth cycle of the voltammogram of steel in HCS+Cl. The positive end of the sweep is different in each condition to prevent localized corrosion, where HCS+Cl represents the most aggressive situation. Table 1 summarizes the position of the main anodic (a) and cathodic (c) peaks, identifying the process to which they can be associated to.

The first cycle in HCS is different to the others because the surface has been recently polished and pre-conditioned at a negative potential [48]. After the second cycle in HCS, three anodic peaks were observed. The position of these peaks could be associated to compounds containing Fe(II) and Fe(III) according to the Pourbaix diagram (Fe/H_2O/carbonated solution) calculated by Reffass et al [39]. The position of these peaks depends on pH [41, 44, 48, 49]. The first peak, at -0.63 V (Ia), corresponds to the formation of Fe(II) species, mainly $Fe(CO_3)$ and $Fe(OH)_2$ [31, 37, 41, 50, 51], as shown by equations 1 to 3:

$$Fe + OH^- \rightarrow Fe(OH)_{ad} + e^- \quad (1)$$

$$Fe + HCO_3^- + OH^- \rightarrow Fe(CO_3) + H_2O + 2\,e^- \quad (2)$$

$$Fe(OH)_{ad} + OH^- \rightarrow Fe(OH)_2 + e^- \quad (3)$$

Fe_3O_4 could also be formed in this potential region, although it becomes more unstable as the OH^- concentration decreases and the carbonate content increases [37, 52]. The peak at -0.44 V (IIa) could be due to the formation of compounds containing Fe(III) [41, 50] according to equations 4 and 5:

$$2\ Fe(OH)_2 + 2\ OH^- \rightarrow Fe_2O_3 + 3\ H_2O + 2\ e^- \quad (4)$$

$$2\ Fe(OH)_2 + 2\ OH^- \rightarrow 2\ FeOOH + 2\ H_2O + 2\ e^- \quad (5)$$

Finally, the peak at -0.24 V (IIIa) could be due to the conversion of $Fe(OH)_2$ into Fe(III) hydroxides or oxo-hydroxides, others than those formed at IIa [48, 50, 51]. After reversing the sweep, two cathodic peaks were observed, corresponding to the reduction of Fe(II) and Fe(III) species. The different species reducing are like to show superimposed broad peaks. When the number of cycles increases, the current density in the passivity region decreases while the intensity of reduction peaks Ic and IIc increases. This behavior could be related to the accumulation of compounds formed in the anodic sweep that are not completely reduced during the cathodic sweep [14, 48].

When testing steel in HCS+Cl (Figure 2a), the first difference to be observed is that the anodic potential needs to be set 500 mV more negative than in HCS to avoid pitting. Also, comparing the anodic peaks in the tenth cycle, it can be seen that peaks Ia and IIa are more intense in HCS+Cl, suggesting that the passivation process is more difficult due to the formation of soluble chlorides. The differences in the cathodic scans are probably due to the more negative reverse potentials. As this limit moves to more positive values, there is more time for the oxides to grow, resulting in higher cathodic currents when they reduce after reversing the sweep direction.

Figure 2b finally shows that when adding biphosphate ions as inhibitor (HCS+I/Cl-1), the potential sweep can again be extended to more positive values. This can be taken as the first signal for the positive effect of the presence of biphosphates. Only two anodic peaks can be identified: Ia at -0.63 V and IIa at -0.35 V, which result in just one cathodic peak during the reverse scan. As in Figure 2a, more than one species might be reducing within one broad peak. No changes can be observed in the position or intensity of the anodic and cathodic peaks when the number of cycles increases. This behavior may be due to the complete reduction during the cathodic sweep of the compounds formed during the anodic sweep. When compared to HCS, the differences may indicate a change in the composition of the passive film. The current density during the anodic sweep in the tenth cycle, is much lower for HCS+I/Cl-1 than for the other two conditions, which suggests a compact and protective surface film, with a different composition from those grown in the absence of biphosphate ions in solution.

The evolution of OCP in time indicates that stable values, typical of passive electrodes, can be attained after keeping the electrodes 24 h at open circuit potential. This is valid for the different electrolytes tested. The stabilized OCP values measured are presented in Tables 2 and 3. Subsequently, electrochemical impedance spectra were recorded to continue the evaluation of surface films formed in contact with various amounts of the inhibiting agent. The results were analyzed using the equivalent circuit presented in Figure 3. This equivalent circuit is representative of oxide-coated metals and has

been chosen before by different authors [13, 35, 36, 53, 54]. Particularly, Ye et al. [55] report in detail why an equivalent circuit with two RC loops is appropriated to analyze EIS spectra corresponding to reinforcement steel in carbonated solutions with various chloride ion concentrations.

Figure 4 displays the Bode representation of the results obtained using HCS, HCS+Cl, HCS+I/Cl+02, HCS+I/Cl+06, and HCS+I/Cl-1. The points represent the actual data, and the lines correspond to a fitting carried out using the equivalent circuit. In this circuit, Rs symbolizes the solution resistance; Ro and ZCPEo the resistance and pseudo-capacitance of the oxide layer, respectively, while Rt and ZCPEt denote the resistance and pseudo-capacitance for charge transfer at the metal surface, respectively. The acronym CPE stands for constant phase element. This is a non-ideal capacitor that better represents the inhomogeneities typical of an oxide layer. The impedance of constant phase elements is given by $Z_{CPE} = [Q(j\omega)^n]^{-1}$, where Q is a constant and n a power, with $-1<n<1$. Cases where $n=1$ represent an ideal capacitor, while $n=0$ corresponds to a pure resistor.

Figure 4 shows that the maximum of the curves is wide, suggesting that there are actually two overlapping maxima. This supports the use of two time-constants in the proposed equivalent circuit and, as does the depressed semi-circle observed in the Nyquist diagram (not shown). In addition, for higher biphosphate contents, the maximum angle is close to 90 degrees. This reflects the capacitive behavior of the oxide film. It can also be observed that the total impedance increases when using HCS+I/Cl-06 and HCS+I/Cl-1. This can be interpreted as a higher polarization resistance and, therefore, it can be associated to a film that is more resistive and protective than those formed using the lowest inhibitor concentration or no inhibitor.

Table 2 summarizes the fitting parameters calculated for each solution. As can be seen, for HCS+I/Cl-06 and HCS+I/Cl-1, ZCPEo is close to 50 $\mu\Omega^{-1}cm^{-2}$ S^N, which is a value typical of passive layers formed on carbon steel in alkaline solutions [13, 48, 56]. Also, n is close to 1. Values higher than 0.9 correspond to a capacitive response, again in agreement with the presence of a protective film [13, 48, 56, 57]. In general, if the four conditions are compared, it can be observed that as the inhibitor content increases, Rt and Ro increase while ZCPEo and ZCPEt decrease. This agrees with the presence of a more protective film where water cannot penetrate [58]Also, Rs is observed to decrease, as expected when the inhibitor content increases and reflecting the increment in the conductivity of the electrolyte. The results in Table 2 also reveal a similar behavior for HCS+Cl and HCS+I/Cl-02, showing little or no effect of the inhibitor present in solution. The highest ZCPEo value (associated to the highest capacitance) corresponds to HCS+I/Cl-02. Usually, an increase in the capacitance can be related to two factors: (1) the passive layer is thinning; and/or (2) the porosity in the electrode surface increases

[55]. Both could explain in increment in the risk of pitting corrosion. In contrast, the better response of the surface film is evident for the conditions with higher dosages: HCS+I/Cl-06 and HCS+I/Cl-1.

The effect of the inhibitor was next tested by performing polarization curves. Figure 5 shows representative results for the anodic polarization curves obtained after keeping the electrodes at OCP for 24 hours. The starting point of each potential sweep is its OCP. Electrochemical parameters such as pitting potential (*Epit*) and passivity current (*i pas*) can be extracted from these curves. The values for OCP, *Epit* and *i pas* shown in Table 3, are averages of not less than 5 experiments for each condition.

Steel remains passive when immersed in HCS, as can be deduced from the extended potential interval where *i pas* is lower than that recorded for HCS-Cl. The potential scan reaches quite positive values and the electrodes do not show pitting, given that in the reverse scan the current is lower than in the forward scan.

The condition with chloride ions and no inhibitor present (HCS-Cl) is the most aggressive one. The curve in this electrolyte shows the highest *i pas* and the most negative or active pitting potential. As expected, this is the condition where polarized steel shows the lowest resistance to localized attack.

An evident improvement can be observed when the inhibitor is incorporated to this solution, even with the lowest inhibitor dosage (HCS+I/Cl-02). There is a clear potential interval where the *i pas* is lower than in the absence of inhibitor. The OCP and *Epit* increase when biphosphate ions are present in solution. However, the samples suffer pitting corrosion and the curves do not show a repassivation potential. This was also the case in solutions with lower carbonate ions content [22]. The inhibitor has a strong influence on the anodic response since the passivity current decreases and the pitting potential increases when the inhibitor dosage increases. This also proofs that the inhibitor efficiency is sensible to concentration increments. A decrease in passive current points to the presence of a passivating film that is either thicker or increasingly compact for higher contents of phosphates. On the other hand, the slightly higher OCP would also be indicative of changes in the composition of the surface layer growing on the metal. Table 3 shows that the pitting potential becomes more positive (more noble) as the amount of inhibiting agent in solution increases. It is also clear that the pitting potential moves away from the open circuit potential (the difference *Epit* - OCP increases), which is taken as indication of less risk of pitting as the inhibitor concentration increases.

The morphology of the metal surface was analyzed after the anodic polarization curves were recorded. Figure 6 shows micrographs of the surface of the electrodes' surface after having removed the red corrosion products. As reported above, all the conditions where chloride ions are present, show localized attack (pitting). As it could be anticipated, the condition where no inhibiting agent is present shows the most severe attack. Visual inspection discarded that the pits were located at the metal/resin

boundary, as this may have indicated crevice corrosion. For the condition HCS+I/Cl-02 the morphology is irregular, with pits of various sizes, some of them interconnected. In the case of HCS+I/Cl-06 the pits are interconnected or ramified. Less pits are detected but bigger than those in HCS+I/Cl-02. This is not unlikely since for these samples the pits had a longer time to grow, given that the sample is not re-passivated, and the potential sweep does not end until the initial potential is reached. Higher *Epit* values, depending on the condition evaluated, result in longer times available for pits growth. Finally, when surveying samples tested using the highest dosage of biphosphate ions (HCS+I/Cl-1), a distinctive behavior can be observed when compared to the previous two conditions. The attack is more localized, with limited corrosion products present. After removing the corrosion products, the pits are found to be bigger in size and shallow. Most of the electrode surface remains free of attack and the difference between this and the other three conditions is notorious. These results confirm that the condition with the highest concentration of biphosphate ions in solution provides a better degree of protection against pitting corrosion.

The samples' surfaces were further analyzed by Raman spectroscopy after recording the anodic polarization curves. When the inhibitor was present, two regions were tested: with and without corrosion products. The bands were assigned according to data collected from different authors [59-63], summarized in Table 4. Figure 7 presents Raman spectra comparing an analysis of the passive film formed in HCS and the corrosion products formed in HCS+Cl. In the case of HCS, the spectrum shows no defined bands that could be associated with oxides present in the passive film. This is probably because the surface film is very thin and cannot be detected by this technique. The monotonous increase in intensity is associated with fluorescence [64]. The spectrum of corrosion products for samples in HCS+Cl is better defined, suggesting thicker or more crystalline films. The position of the bands indicates the presence of α-FeOOH, which is consistent with the reddish appearance of corrosion products observed in this condition.

Figure 8 shows the spectra corresponding to the condition HCS+I/Cl-06 analyzing two spots: one with corrosion products on the surface and another free of them. In the region with corrosion products, a wide peak between 900 and 1200 cm^{-1} was observed. This wide peak is associated to the presence of the characteristic PO_4^{-3} / HPO_4^{-2} triplet, where the bands are widened due to amorphous corrosion products. In this region, the most intense band of $FeCO_3$ is also located at 1080 cm^{-1}, which may overlap with the phosphate bands. When the surface attack starts, the morphology and precipitate type depend on the composition of the solution [61]. Several authors have proposed the formation of an unstable precipitate commonly known as "Green Rust (GR)" [38, 61, 65, 66]. These oxides include Fe(II) and/or Fe(III) and anions such as OH^-, Cl^- and CO_3^{-2}. Refait and col. [65] concluded that GR(CO_3^{-2}) is not formed when phosphates are present simultaneously with Fe(II), hydroxyls and bicarbonate ions.

The broadband between 600 and 800 cm^{-1} can be attributed to the participation of amorphous oxo-hydroxides containing Fe(III) [65, 66]. It can also be seen that the Raman spectrum for the region without corrosion products presents a signal with no distinctive features. This could be because the passive film is thin, and the technique is not sensitive enough.

In the case of electrodes where the polarization curve was carried out in HCS+I/Cl-02, it can be observed that the spectra are quite like the case shown in Figure 8. The broadband between 600 and 800 cm^{-1} is slightly more intense while the peak between 900 and 1200 cm^{-1} is a bit less intense. This tendency is confirmed for condition HCS+I/Cl-1, where the band between 600 and 800 cm^{-1} can hardly be identified, while the one between 900 and 1200 cm^{-1} dominates the spectrum. This can be taken as indication of biphosphate ions incorporating into the corrosion products. For these two dosages, the spectrum corresponding to the area without corrosion products remains without distinctive features.

The inhibition efficiency was also tested over several weeks of immersion. Coupons were evaluated in the five conditions considered in the present work. Figure 9 presents images showing the surfaces after 42 days of immersion in the solutions containing chloride ions. Big differences can be appreciated in terms of the extent of attack. An important amount of corrosion products appears on the surface of those coupons immersed in HCS+Cl and in HCS+I/Cl-02. In contrast, no attack was detected for the samples immersed in HCS+I/Cl-06 and HCS+I/Cl-1. Quantitative results are presented in Table 5. The inhibition percentage was calculated using the following equation, (eqn. 6):

$$\%\zeta = \left[1 - \frac{W_{\text{with inhibitor}}}{W_{\text{without inhibitor}}}\right] x100 \qquad (6)$$

The corrosion current density (*i corr*) presented in Table 5 was calculated using Faraday's law (see eqn. 7)

$$i\,corr = \frac{W\ F}{A\,t\,eq} \qquad (7)$$

where A is the exposed geometrical area, W is the mass lost, F represents the Faraday constant, t is the immersion time and eq is the equivalent weight (taking here that of iron, eq= 27.92 g/mol). HCS is considered as the reference situation, where weight loss values are insignificant. The opposite is evident in HCS+Cl. The inhibitory effect of biphosphate ions is clear, even in the lower dosage. The inhibition efficiency improves markedly as the amount of biphosphate increases. The two highest dosages show a negligible mass lost. In both these cases, no sign of localized attack was detected. Also, the calculated values for the corrosion current density in HCS+I/Cl-06 and HCS+I/Cl-1 are

typical of passive steel, even if the coupons have been immersed for six weeks in chloride-containing electrolytes.

The composition of passive films naturally developed at OCP for 7 days in aerated solutions were analyzed by XPS. The results are shown in Figure 10, presenting the peaks corresponding to O1s, $Fe2p_{3/2}$, and P1s. These signals were deconvoluted and the results can be seen in Table 6.

First, O1s is analyzed. In the case of HCS, three contributions can be observed. The one at 530 eV is associated to the presence of Fe_2O_3 and Fe_3O_4 [22, 48, 67] and that at 531 eV is related to the presence of hydroxides [22, 67]. The contribution at 532.9 eV had been related before to the participation of CO_3^{2-} in the passive film [35, 68]. The signals at 531 and 532.9 eV are not observed in HCS+Cl, indicating that the passive film is mainly composed by oxides when chloride ions are present. In HCS+I/Cl-1, although the passive film is mainly composed by hydroxides (63.5%), phosphate participation was detected at 532 eV. The participation of phosphate ions in the passive film can be confirmed by the presence of P2p peak at 132.5 eV [27, 69] (see Figure 11).

The Fe2p3/2 peak deconvolution is also presented in Figure 10. In agreement with previous work, the contributions related to the presence of Fe^0, Fe(II) and Fe(III) compounds are observed at 706.7, 709.6 and 711 eV, respectively [67, 70, 71]. It is evident that in HCS, Fe(II) compounds are the predominant species, although in HCS+Cl and HCS+I/Cl-1, the contribution of Fe(III) compounds to the composition of the passive film increases. In HCS and HCS+Cl, no Fe^0 contribution can be observed. Even if the thickness cannot be calculated in these two cases, this suggests that the passive film thickness is higher than 10 nm in these two cases, while the film is thinner when the inhibitor is present. The values in Table 6 can be used to calculate the film thickness only in the case of HCS+I/Cl-1, assuming uniform coverage over the entire surface, and following the work by Ghods and col. [67]. Fe^{OX} is calculated as the contribution from Fe(II) and Fe(III) peaks in Table 6. Following the calculation explained in detail elsewhere [67], the thickness of the surface film (dox) can be calculated resulting in 5.28 nm.

Discussion

The effect of phosphate contents on steel corrosion in carbonated solutions contaminated with chloride ions will be discussed taking as reference the results in HCS. Most of the electrochemical evaluation was carried out after stabilizing the OCP for 24 hs prior to testing. The results suggest that in the long term, a pre-passivation layer grown in alkaline solution would have probably made little or no

difference. The effect of the carbonate content will be evaluated by comparison with previous results, using solutions with a lower carbonate content [22].

When the carbonate content was high (0.015 mol L^{-1} Na_2CO_3 and 0.3 mol L^{-1} $NaHCO_3$, in HCS), steel remained passive, even at pH=9. Anodic polarization curves showed extremely low passivity current values and no localized attack, in agreement with previous studies [31, 33, 41, 43, 45]. XPS analysis of the naturally grown passive film, indicated that it is thicker than 10 nm and mainly composed by $FeCO_3$ with minor contributions of Fe_3O_4 and Fe_2O_3. After 6 weeks of immersion, weight loss was negligible. In parallel, steel samples were evaluated after adding chloride ions to the HCS solution. Cyclic voltammograms enabled a rapid characterization of the first stages in the surface film formation in deaerated solutions. Higher currents were observed in the voltammograms and attributed to the presence of a more unstable surface film when chloride ions are present. Polarization curves showed localized attack, higher passivation currents and low pitting potentials, with no repassivation. Microscopic images showed big, irregular, and ramified pits. EIS results from films formed by 24 h immersions were consistent with the development of a less protective surface film. XPS analysis of films developed for 7 days suggested that the film is thicker than 10 nm and mainly composed of Fe_3O_4 and Fe_2O_3. After 6 weeks of immersion in HCS+Cl, weight loss was maximum. The stability of the surface layer was compromised due to a competition between chloride, hydroxyl, and carbonate ions adsorption. As it has been shown before [45, 72], chloride ions move faster than hydroxyl and carbonate ions. Both, ferric and ferrous chlorides are much more soluble than ferric and ferrous hydroxides and carbonates. Thus, it can be argued that when chloride ions are present, less adsorbed $FeCO_3$ is produced. In contrast, $Fe(Cl)_{ad}$ forms, which can be readily dissolved and oxidized into ferrous and ferric chlorides and may explain the high value for the weight loss reported in Table 5.

Biphosphate ions were tested as inhibiting agents. To better understand this inhibition process, the incorporation of biphosphate ions, three dosages were investigated: biphosphate/chloride=0.2, 0.6, and 1. While carrying out cyclic voltammograms with biphosphate/chloride=1, lower anodic currents were detected, and the potential window could be extended to more positive values. The surface layer became more protective, and the composition of the passive film changed accordingly. This was a first indication of biphosphate ions behaving as promising inhibiting agents. Then, EIS results showed a clear improvement in the quality of the passive film when the inhibitor content increased. However, the lowest dosage (HCS+Cl/I-02) showed almost no difference when compared to HCS+Cl. Yet, as the biphosphate concentration increased, the results became those typical of protective layers, showing higher values of charge transference resistance, and behaving as a more protective films [22, 44, 56]. In anodic polarization tests, when the inhibitor was present, the passivity current was lower than in HCS+Cl. In parallel, the pitting potential increased and the OCP became more anodic for higher

biphosphate dosages. Yet, the samples still suffered localized corrosion with no evidence of re-passivation. The morphology of the pits when the inhibitor and chloride ions were simultaneously present revealed that higher inhibitor dosages promoted bigger and shallow pits. XPS results indicated that in HCS+I/Cl-1, a thinner protective passive film is formed, more compact than those grown in HCS+Cl. This passive film is mainly composed by Fe(III) oxide/hydroxide, with a minor contribution of biphosphate compounds, in agreement with previous results from other authors [24, 25, 38]. When evaluated over a prolonged period, the differences in the mass lost are significant, particularly for the intermediate and highest inhibitor dosages. The differences between the surface layer comparing the three electrolytes under investigation are represented schematically in Figure 12.

Moreover, it is important to stress again that pH values as well as hydroxyl/carbonate ratios together with the total amounts of these two ions are factors that strongly influence the stability of the passive film on steel [31, 33, 37, 38]. In previous studies, the effect of phosphate ions was investigated at pH=9 using inhibitor/chloride ratios = 0.2, 0.6 and 1, but with ten times less carbonation (LCS, ($[HCO_3^-] + [CO_3^=]$) = 0.0315 mol L^{-1}) [22]. Results using pore solutions extracted under pressure from carbonated concrete, in accelerated laboratory tests, have indicated that LCS better simulates carbon steel corrosion in carbonated concrete [73-75]. However, a highly carbonated solution (HCS) better represents an environment where the CO_2 content is higher than that in the atmosphere for many years, such as underground parking lots or certain industrial facilities. The influence of the carbonate content is frequently neglected in the literature, generally assuming that a pH value close to 9 in enough to simulate carbonate concrete. However, not all the real situations that lead to carbonation can be taken as equivalent.

The carbonatation level is found to influence the surface film composition. At pH=9, steel actively corroded in solutions with low amounts of carbonate ions [22]. It has to be taken into account that the carbonate/bicarbonate buffer solution is relatively diluted and it has a low capacity to regulate the acidification processes that result from iron oxidation (see equations 1 to 5) [20]. Passivity could be regained using biphosphate ions as inhibiting agents but only when the relation chloride/inhibitor was 1. In that case, phosphate ions incorporated to the passive film by a dissolution-precipitation mechanism that initially formed $Fe_3(PO_4)_2$, which then lead to a mixture of Fe(II)/Fe(III) phosphates and oxides. In contrast, steel remained passive in highly carbonated solutions. The first stage in the film growth could be the formation of a protective layer of $FeCO_3$. This passivity is compromised by the presence of chloride ions, which adsorb and promote the dissolution of iron as ferrous and ferric chlorides. This loss of passivity can be compensated by the addition of biphosphate ions. Even when incorporated to a highly carbonated solution contaminated with chloride ions, the presence of biphosphate ions has a positive inhibitory effect that depends on its concentration. Phosphate and

biphosphate ions are known to favor the oxidation of Fe(II) ions [38] promoting the development of a passive film rich Fe(III) hydroxides. The role of phosphates could also be to compete with chloride ions via the absorption mechanism of ligand exchange proposed by Chitrakar et al. [76] and to inhibit the film destabilization observed in HCS-Cl. This would prevent the migration and dissolution by chloride complex formation and improve protectiveness, resulting in the development of passive oxides and/or hydroxides. The inhibitory effect of phosphates is sensitive to its concentration, both in LCS and in HCS.

In HCS, there was a noticeable improvement for the condition HCS+Cl/I-06, as compared to HCS+Cl/I-02, with no big differences between this and the addition of higher amounts of inhibitor (HCS+Cl/I-1). It could then be cost-effective to choose this intermediate dosage (HCS+Cl/I-06) as the optimal concentration to achieve safe-enough corrosion control in locations where high concentrations of CO_2 may be present, such as closed parking lots. A follow-up study using mortars instead of simulating solutions will be necessary to confirm these auspicious results.

Combining these results with those from previous studies, a broad range of carbonate and biphosphate contents can be analyzed [22]. A linear relationship was found between (*Epit* -OCP) and $\log([HPO_4^{2-}]\cdot([CO_3^{2-}] + [HCO_3^-]/[Cl^-]))$ (see Table 3). The results are presented in Figure 13. This could be useful to estimate the risk of pitting when the carbonation degree and the concentration of biphosphate and chloride ions are different from those used in the reported investigations.

Conclusions

- Even at pH=9, steel remains passive in solutions when the concentrations of carbonate ions are as high as 0.015 mol L^{-1} Na_2CO_3 and 0.3 mol L^{-1} $NaHCO_3$,(HCS). Mildly alkaline pH values are not enough to simulate rebar corrosion in carbonated concrete.
- In aerated HCS, the passive film on steel is composed of a mixture of oxides and carbonates. By adding chlorides to the solution, the composition of the surface film changes, passivity is lost, and localized attack cannot be prevented. However, the incorporation of biphosphate ions to the carbonated solution contaminated with chloride ions modifies the chemical composition of the passivating film. The resistance against localized corrosion improves and pitting can be inhibited.

- In carbonated solutions, the response of the system to the presence of the inhibiting agent depends on the content of biphosphate ions in solution, indicating that proper dosages must be considered.

- In solutions with Na_2CO_3 0.015 mol/L and $NaHCO_3$ 0.3 mol/L contaminated with NaCl 0.1 mol/L, the optimal dosage of Na_2HPO_4 is 0.06 mol/L. Even when evaluated for several weeks, the effect is comparable to that obtained using 0.1 mol/L of Na_2HPO_4 but with the advantage of needing a lower amount of inhibitor.

- Using pore simulating solutions with a pH value fixed in 9 and NaCl 0.1 mol/L, the total carbonate content determines the response of steel against corrosion. Key factors such as the passive or active behavior, the pitting potential, the surface layer composition and the minimum amount of inhibitor required to guarantee an adequate protection against corrosion, among others, depend on the carbonation level.

- A linear relationship was found between (*Epit* -OCP) and log ($[HPO_4^{2-}]\cdot([CO_3^{2-}] + [HCO_3^-]/[Cl^-])$) which could be useful to estimate the risk of pitting when the carbonation degree and the concentration of biphosphate and chloride ions are different from those used in the reported investigations.

- The viability of using Na_2HPO_4 in cost-effective concentrations as an efficient corrosion inhibitor is demonstrated when tested in pore solutions that simulate a heavily carbonated concrete contaminated with chloride ions, which could be useful under specific service conditions.

Acknowledgments

The authors would like to recognize the financial support provided by the University of Mar del Plata (Grant 15/G598), and the Agencia Nacional de Promoción Científica y Tecnológica (grant PICT 2392/18).

References

1. C. L. Page and K. W. J. Treadaway, *Nature*, **297** (5862), 109-115 (1982).
2. K. Tuuti, *Corrosion of Steel in Concrete*, Sweedish Cement and Concrete Research Institute (1982).
3. S. W. Tang, Y. Yao, C. Andrade, and Z. J. Li, *Cement and Concrete Research*, **78** 143-154 (2015).
4. A. S. Al-Ameeri, M. I. Rafiq, and O. Tsioulou, *Cement and Concrete Composites*, **115** (2021).
5. G. K. Glass and N. R. Buenfeld, *Corrosion Science*, **39** (5), 1001-1013 (1997).
6. H. Nahali, L. Dhouibi, and H. Idrissi, *Construction and Building Materials*, **50** 87-94 (2014).
7. G. R. Meira, C. Andrade, E. O. Vilar, and K. D. Nery, *Construction and Building Materials*, **55** 289-298 (2014).
8. H. Saricimen, M. Mohammad, A. Quddus, M. Shameem, and M. S. Barry, *Cement and Concrete Composites*, **24** (1), 89-100 (2002).
9. V. Saraswathy and H. W. Song, *Building and Environment*, **42** (1), 464-472 (2007).
10. T. A. Söylev and M. G. Richardson, *Construction and Building Materials*, **22** (4), 609-622 (2008).
11. A. Tiwari, S. Goyal, V. Luxami, M. K. Chakraborty, and G. Prabhakar, *Construction and Building Materials*, **290** (2021).
12. N. Etteyeb, L. Dhouibi, H. Takenouti, M. C. Alonso, and E. Triki, *Electrochimica Acta*, **52** (27 SPEC. ISS.), 7506-7512 (2007).
13. M. B. Valcarce and M. Vázquez, *Electrochimica Acta*, **53** (15), 5007-5015 (2008).
14. L. Yohai, M. Vázquez, and M. B. Valcarce, *Electrochimica Acta*, **102** 88-96 (2013).
15. S. Toujas, M. Vázquez, and M. B. Valcarce, *Corrosion Science*, **128** 94-99 (2017).
16. S. Muralidharan, V. Saraswathy, K. Thangavel, and S. Srinivasan, *Journal of Applied Electrochemistry*, **30** (11), 1255-1259 (2000).
17. S. M. Abd El Haleem, S. Abd El Wanees, E. E. Abd El Aal, and A. Diab, *Corrosion Science*, **52** (2), 292-302 (2010).
18. H. Verbruggen, H. Terryn, and I. De Graeve, *Construction and Building Materials*, **124** 887-896 (2016).
19. Y. Q. Wang, G. Kong, C. S. Che, and B. Zhang, *Construction and Building Materials*, **162** 383-392 (2018).
20. M. Reffass, R. Sabot, M. Jeannin, C. Berziou, and P. Refait, *Electrochimica Acta*, **54** (18), 4389-4396 (2009).

21. L. Yohai, W. Schreiner, M. B. Valcarce, and M. Vázquez, *Journal of the Electrochemical Society*, **163** (13), C729-C737 (2016).
22. L. Yohai, W. Schreiner, M. Vázquez, and M. B. Valcarce, *Electrochimica Acta*, **202** 231-242 (2016).
23. H. S. Lee, H. M. Yang, J. K. Singh, S. K. Prasad, and B. Yoo, *Construction and Building Materials*, **173** 443-451 (2018).
24. A. Mohagheghi and R. Arefinia, *Construction and Building Materials*, **187** 760-772 (2018).
25. S. Mandal, J. K. Singh, D. E. Lee, and T. Park, *Materials*, **13** (16), 3462 (2020).
26. L. Yohai, M. B. Valcarce, and M. Vázquez, *Electrochimica Acta*, **202** 316-324 (2016).
27. D. Wang, C. Pan, Z. Liu, K. Chen, N. Chen, and S. Liu, *Construction and Building Materials*, **286** (2021).
28. D. Wang, J. Ming, and J. Shi, *Corrosion Science*, **174** 108830 (2020).
29. N. Etteyeb, L. Dhouibi, H. Takenouti, and E. Triki, *Cement and Concrete Composites*, **55** 241-249 (2015).
30. V. Konovalova and V. Rumyantseva, **890** (1), (2020).
31. M. Moreno, W. Morris, M. G. Alvarez, and G. S. Duffo, *Corrosion Science*, **46** (11), 2681-2699 (2004).
32. H. Yu, K. T. K. Chiang, and L. Yang, *Construction and Building Materials*, **26** (1), 723-729 (2012).
33. R. Liu, L. Jiang, J. Xu, C. Xiong, and Z. Song, *Construction and Building Materials*, **56** 16-20 (2014).
34. G. Liu, Y. Zhang, Z. Ni, and R. Huang, *Construction and Building Materials*, **115** 1-5 (2016).
35. Y. Zhao, T. Pan, X. Yu, and D. Chen, *Corrosion Science*, **158** (2019).
36. J. Ming, M. Wu, and J. Shi, *Cement and Concrete Composites*, **123** (2021).
37. M. C. Alonso and M. C. Andrade, *Corrosion Science*, **29** (9), 1129-1139 (1989).
38. J. M. R. Génin, L. Dhouibi, P. Refait, M. Abdelmoula, and E. Triki, *Corrosion*, **58** (6), 467-478 (2002).
39. M. Reffass, R. Sabot, C. Savall, M. Jeannin, J. Creus, and P. Refait, *Corrosion Science*, **48** (3), 709-726 (2006).
40. A. Steffens, D. Dinkler, and H. Ahrens, *Cement and Concrete Research*, **32** (6), 935-941 (2002).
41. B. Huet, V. L'Hostis, F. Miserque, and H. Idrissi, *Electrochimica Acta*, **51** (1), 172-180 (2005).
42. E. B. Castro, J. R. Vilche, and A. J. Arvia, *Corrosion Science*, **32** (1), 37-50 (1991).
43. M. Goldman, C. Tully, J. J. Noël, and D. W. Shoesmith, *Corrosion Science*, **169** (2020).

44. M. B. Valcarce and M. Vázquez, *Materials Chemistry and Physics*, **115** (1), 313-321 (2009).
45. M. B. Valcarce, C. López, and M. Vázquez, *Journal of the Electrochemical Society*, **159** (5), C244 (2012).
46. D. L. Graf, *Clays and Clay Minerals*, **28** (4), 319-319 (1980).
47. A. S. o. T. a. Materials, Vol. ASTM D2688. American Society of Testing and Materials, Philadelphia, U.S.A., 1993.
48. W. Xu, K. Daub, X. Zhang, J. J. Noel, D. W. Shoesmith, and J. C. Wren, *Electrochimica Acta*, **54** (24), 5727-5738 (2009).
49. M. Pourbaix, *Corrosion Science*, **14** (1), 25-82 (1974).
50. L. J. Simpson and C. A. MeIendres, *Journal of Electrochemistry Society*, **143** (7), 2146-2152 (1996).
51. M. Jeannin, D. Calonnec, R. Sabot, and P. Refait, *Electrochimica Acta*, **56** (3), 1466-1475 (2011).
52. L. Freire, M. A. Catarino, M. I. Godinho, M. J. Ferreira, M. G. S. Ferreira, A. M. P. Simões, and M. F. Montemor, *Cement and Concrete Composites*, **34** (9), 1075-1081 (2012).
53. P. Xu, J. Zhou, G. Li, P. Wang, P. Wang, F. Li, B. Zhang, and H. Chi, *Construction and Building Materials*, **288** (2021).
54. D. Wang, J. Ming, and J. Shi, *Corrosion Science*, **174** (2020).
55. C.-Q. Ye, R.-G. Hu, S.-G. Dong, X.-J. Zhang, R.-Q. Hou, R.-G. Du, C.-J. Lin, and J.-S. Pan, *Journal of Electroanalytical Chemistry*, **688** 275-281 (2013).
56. M. B. Valcarce, C. López, and M. Vázquez, *Journal of the Electrochemical Society*, **159** (5), C244-C251 (2012).
57. M. E. Folquer, S. B. Ribotta, S. G. Real, and L. M. Gassa, *Corrosion*, **58** (3), 240-247 (2002).
58. C. Liu, Q. Bi, A. Leyland, and A. Matthews, *Corrosion Science*, **45** (6), 1257-1273 (2003).
59. D. L. A. de Faria, S. Venancio Silva, and M. T. de Oliveira, *JOURNAL OF RAMAN SPECTROSCOPY*, **28** 873-878 (1997).
60. M. S. Odziemkowski, T. T. Schuhmacher, R. W. Gillham, and E. J. Reardon, *Corrosion Science*, **40** (2-3), 371-389 (1998).
61. S. Simard, M. Odziemkowski, D. E. Irish, L. Brossard, and H. Ménard, *Journal of Applied Electrochemistry*, **31** 913-920 (2001).
62. A. Hugot-Le Goff, J. Flis, N. Boucherit, S. Joiret, and J. Wilinski, *Journal of the Electrochemical Society*, **137** (9), 2684-2690 (1990).
63. J. K. Singh and D. D. N. Singh, *Corrosion Science*, **56** 129-142 (2012).
64. D. Wei, S. Chen, and Q. Liu, *Applied Spectroscopy Reviews*, **50** (5), 387-406 (2015).

65. P. Refait, M. Reffass, J. Landoulsi, R. Sabot, and M. Jeannin, *Colloids and Surfaces A: Physicochemical and Engineering Aspects*, **299** (1-3), 29-37 (2007).
66. M. Jeannin, D. Calonnec, R. Sabot, and P. Refait, *Electrochimica Acta*, **56** (3), 1466-1475 (2011).
67. P. Ghods, O. B. Isgor, J. R. Brown, F. Bensebaa, and D. Kingston, *Applied Surface Science*, **257** (10), 4669-4677 (2011).
68. J.K. Heuer and J. F. Stubbins, *Corrosion Science*, **41** 1231-1243 (1999).
69. J.F. Moulder and J. Chastain, *Handbook of X-ray Photoelectron Spectroscopy: A Reference Book of Standard Spectra for Identification and Interpretation of XPS*, p. 261 (1995).
70. M. A. Frontini, W. Schreiner, M. Vázquez, and M. B. Valcarce, *Construction and Building Materials*, **227** (2019).
71. L. Q. Guo, M. C. Lin, L. J. Qiao, and A. A. Volinsky, *Corrosion Science*, **78** 55-62 (2014).
72. Z. H. Dong, W. Shi, and X. P. Guo, *Corrosion Science*, **53** (4), 1322-1330 (2011).
73. D. J. Anstice, C. L. Page, and M. M. Page, *Cement and Concrete Research*, **35** (2), 377-383 (2005).
74. S. Sawada, J. Kubo, C. L. Page, and M. M. Page, *Corrosion Science*, **49** (3), 1186-1204 (2007).
75. M. Hren, T. Kosec, and A. Legat, *Materials and Corrosion*, **71** (5), 759-766 (2020).
76. R. Chitrakar, S. Tezuka, A. Sonoda, K. Sakane, K. Ooi, and T. Hirotsu, *Journal of Colloid and Interface Science*, **298** (2), 602-608 (2006).

Legends

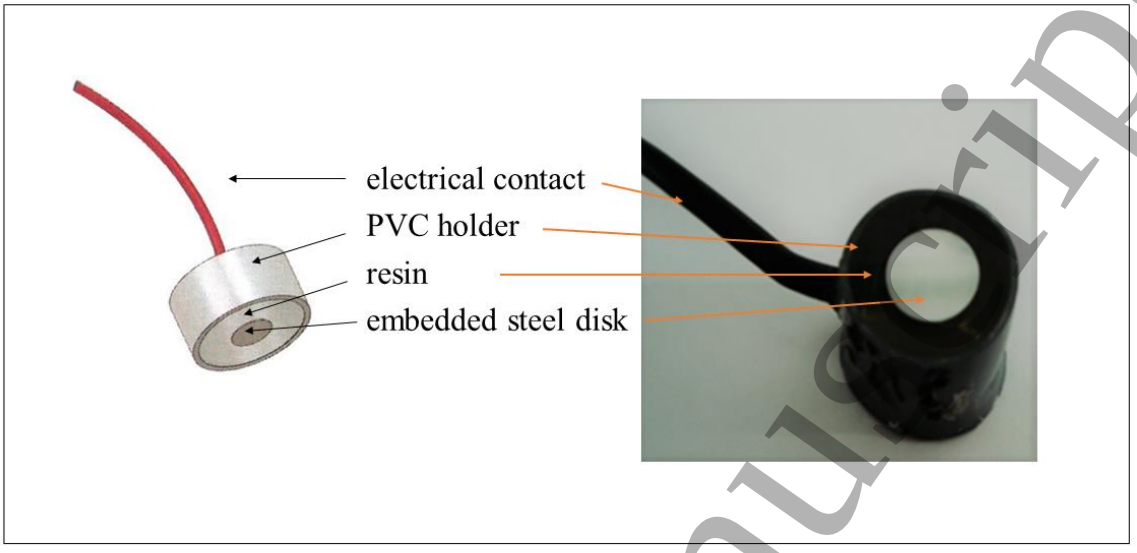

Figure 1: Scheme (left) and photograph (right) of the electrodes used for the electrochemical measurements

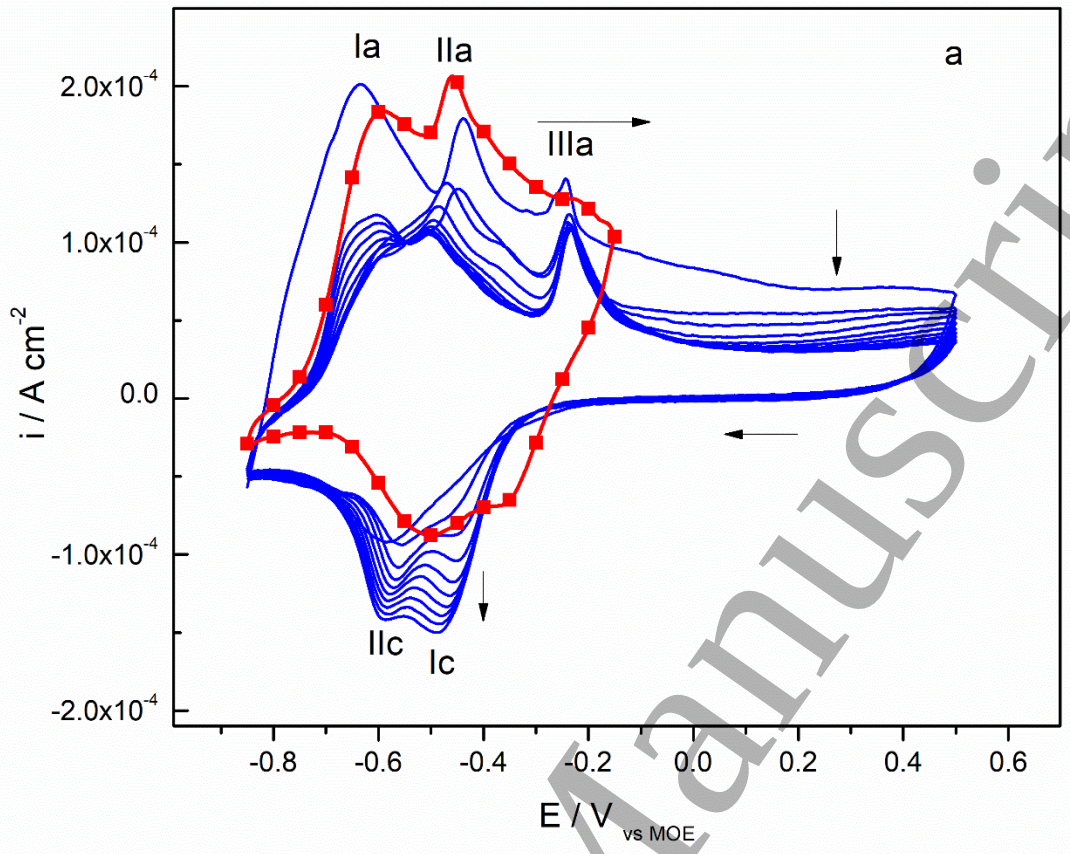

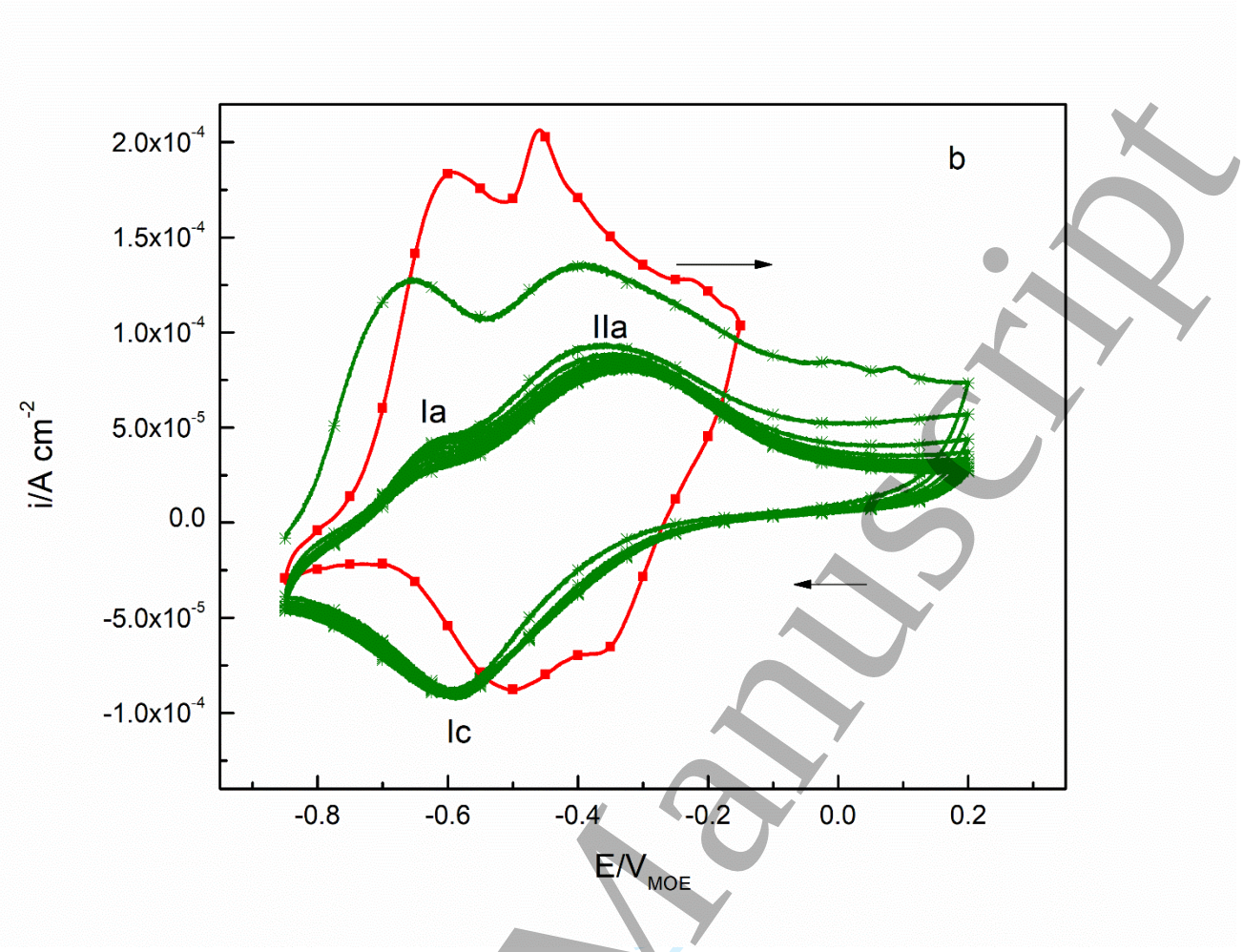

Figure 2. Voltammogram (tenth cycle) performed in HCS+Cl (—■—), together with a) the ten cycles in HCS (—●—) and b) the ten cycles in HCS+I/Cl-1 (—★—). The scan started in the negative end and proceeded at 10 mV s^{-1}.

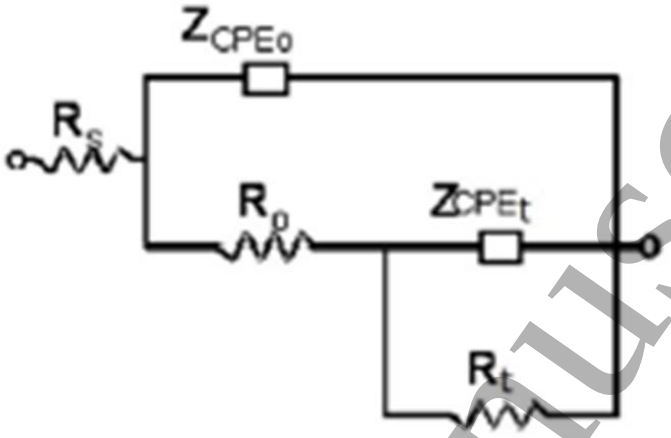

Figure 3. Equivalent circuit representative of oxide-coated metals [13, 35, 36, 53, 54]. Rs represents the solution resistance; Ro and ZCPEo the resistance and pseudo-capacitance of the oxide layer, respectively, and Rt and ZCPEt denote the resistance and pseudo-capacitance for charge transfer at the metal surface, respectively.

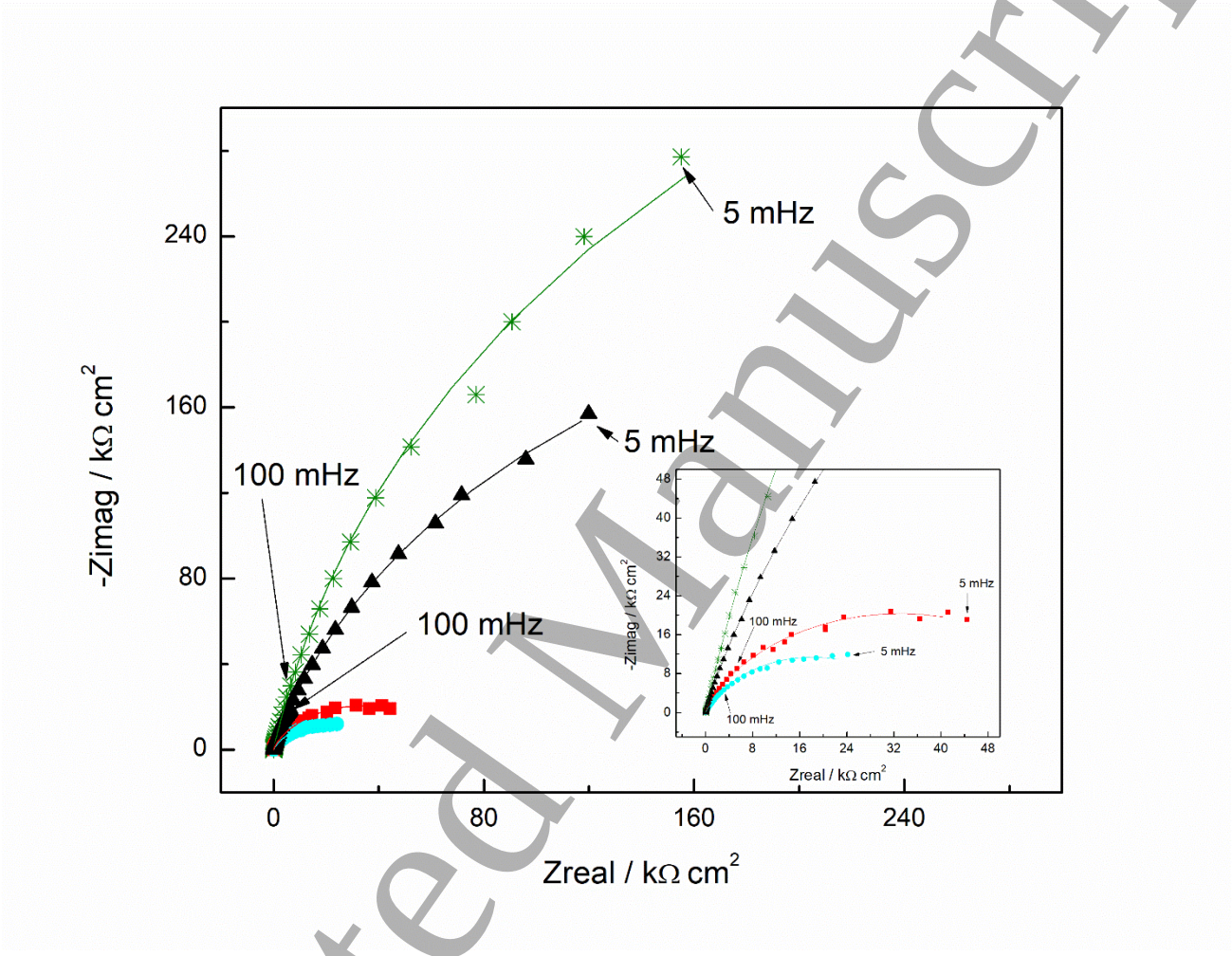

Figure 4. Impedance spectra and fit results for steel aged 24 h at OCP, evaluated in the following conditions: HCS+Cl —■—; HCS+I/Cl-1 —★—; HCS+I/Cl-06 —▲—; HCS+I/Cl-02 —●—. The electrodes were kept at OCP during the scan. The frequency sweep ranged from 20 kHz to 5 mHz, with an amplitude of 10 mV_{rms}. Some frequencies of interest are labeled.

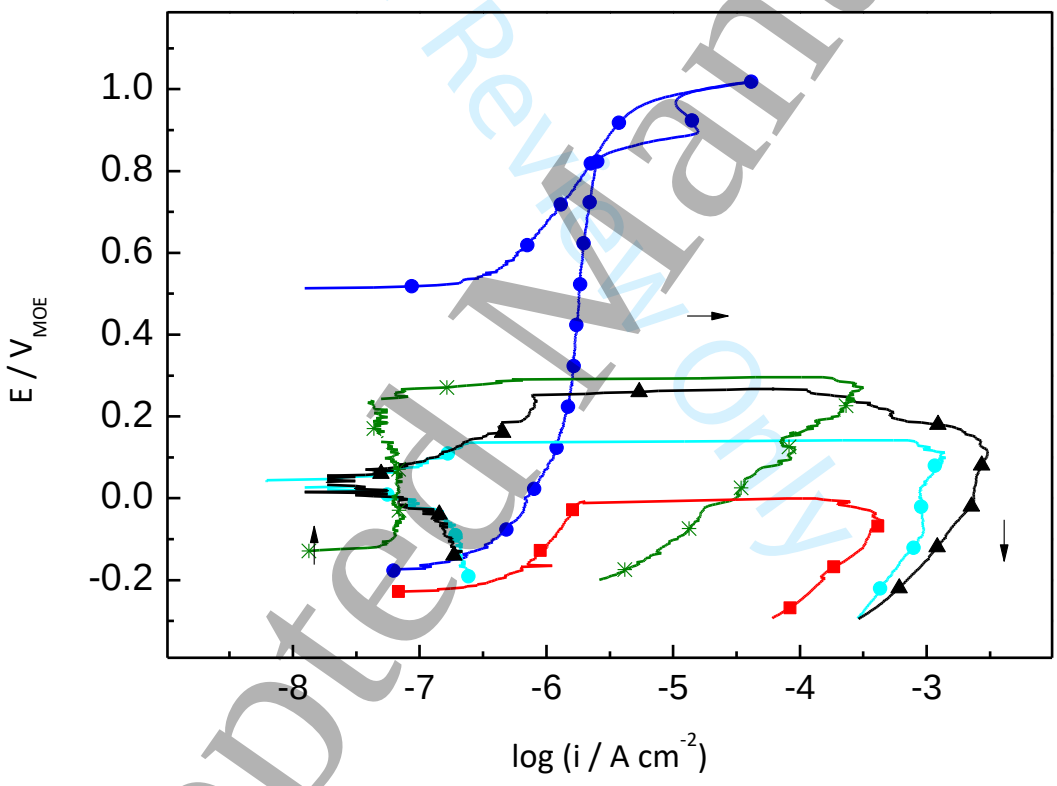

Figure 5. Anodic polarization curves registered after keeping the electrodes for 24 h at OCP. The potential sweep started at OCP with rate of 10 mV s^{-1}. The scan was reversed at 40 µA cm^{-2}. The following electrolytes were tested: HCS —●— ; HCS+Cl —■—; HCS+I/Cl-1 —★—; HCS+I/Cl-06 —▲—; HCS+I/Cl-02 —○—.

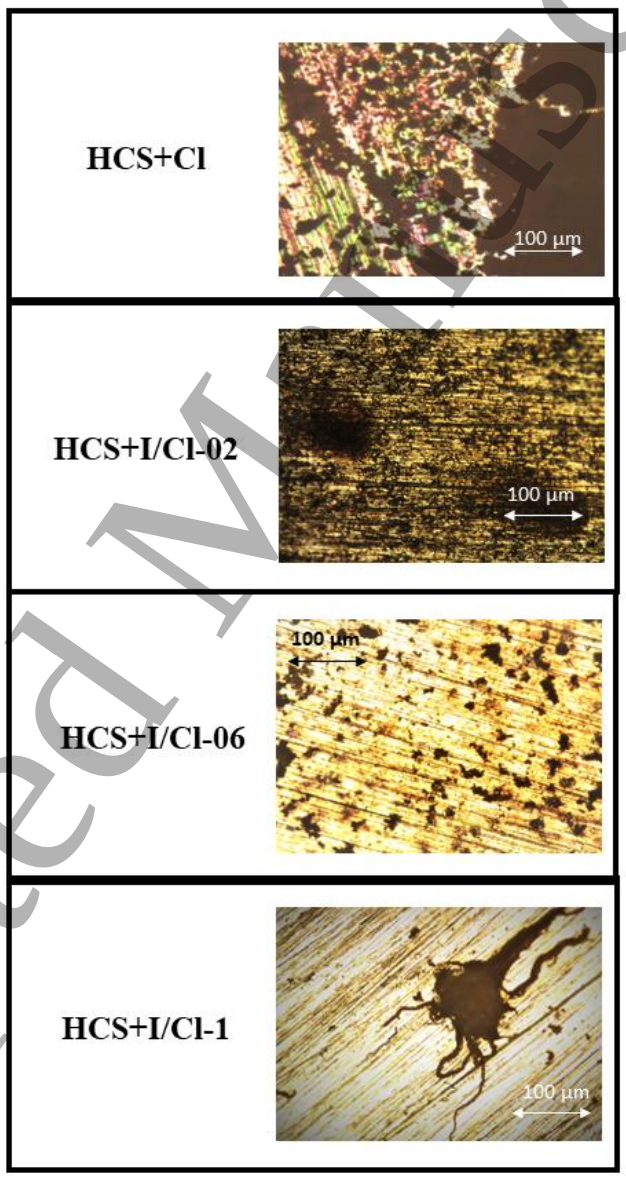

Figure 6. Images of the electrodes after carrying out the anodic polarization curves in the different solutions used in this study. Magnification 100X.

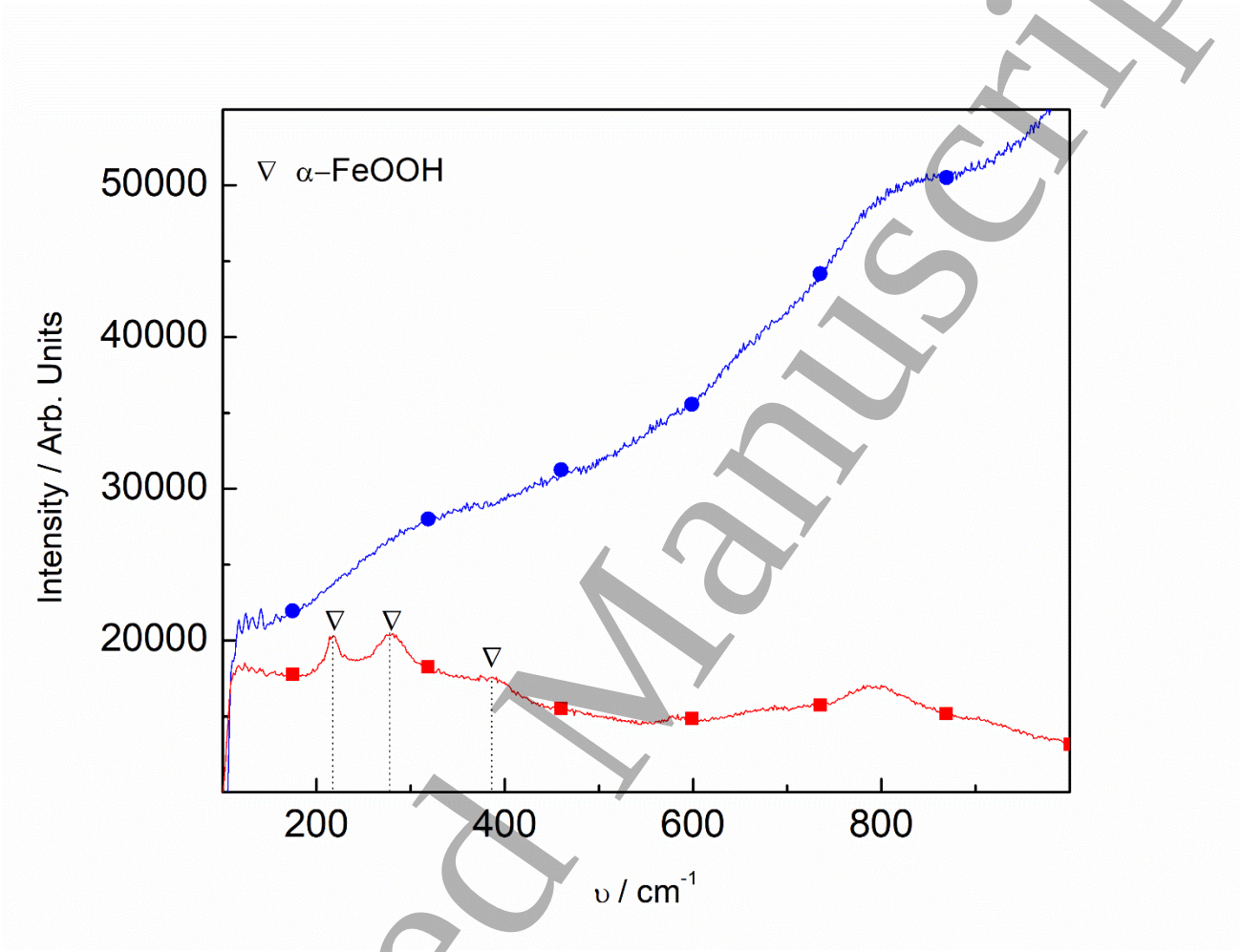

Figure 7. Raman spectra recorded using a 514 nm laser, with 50 s of exposure, at 100% of intensity and a 50X objective. The analysis was undertaken after running anodic polarization curves in HCS (passive film) —●— and HCS+Cl (corrosion products) —■—.

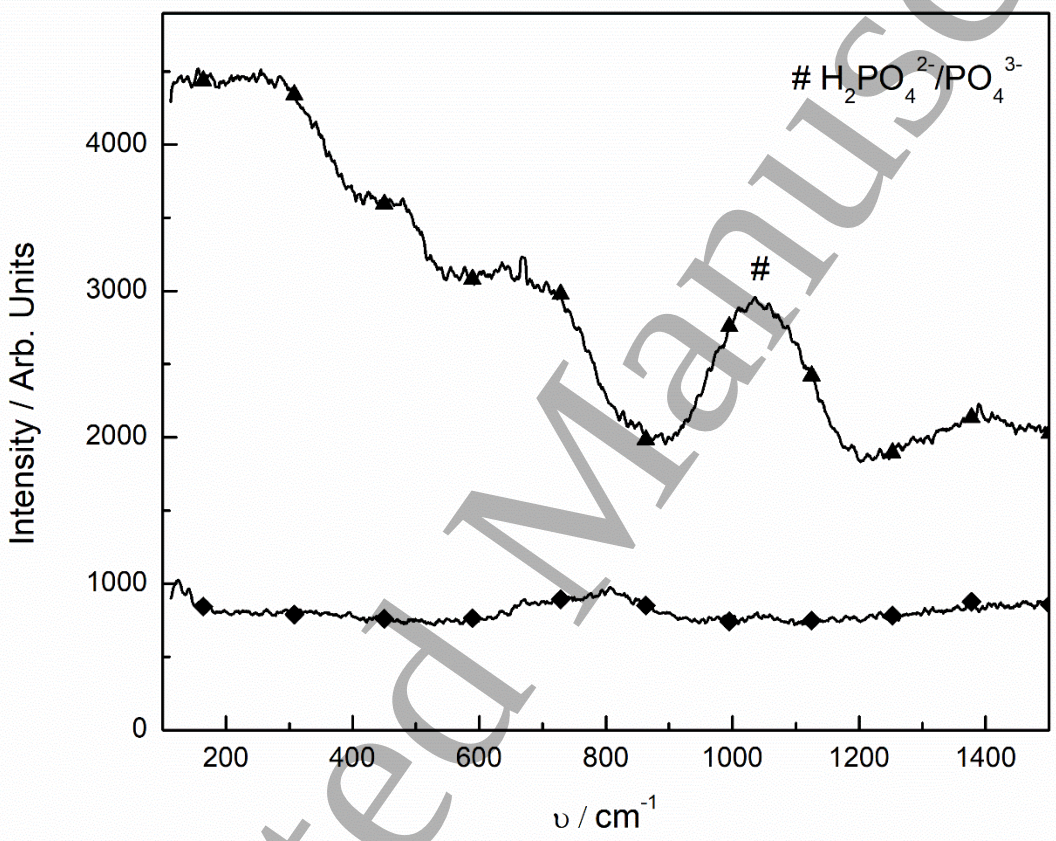

Figure 8. Raman spectra recorded using a 514 nm laser, with 50 s of exposure, at 100% of intensity and a 50X objective. The analysis was undertaken after running anodic polarization curves in HCS+I/Cl-06. Region with corrosion products —▲—; region without corrosion products —♦—.

Figure 9. Photographs of the coupons after 6 weeks of immersion in each of the electrolytes used in this study.

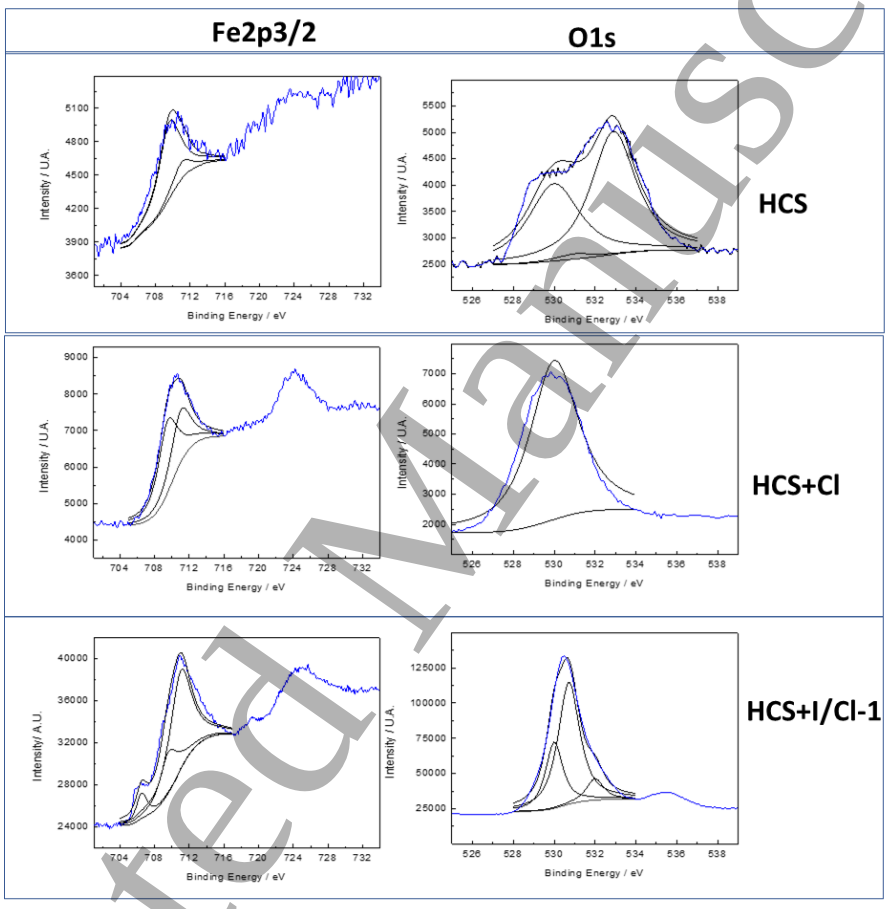

Figure 10. Fe2p3/2 and O1s XPS spectra for passive layers grown on steel for 192 h at OCP. Survey spectra between 0 and 1100 eV binding energy (B.E.) were recorded with 0.1 eV steps and a bandpass of 50 eV.

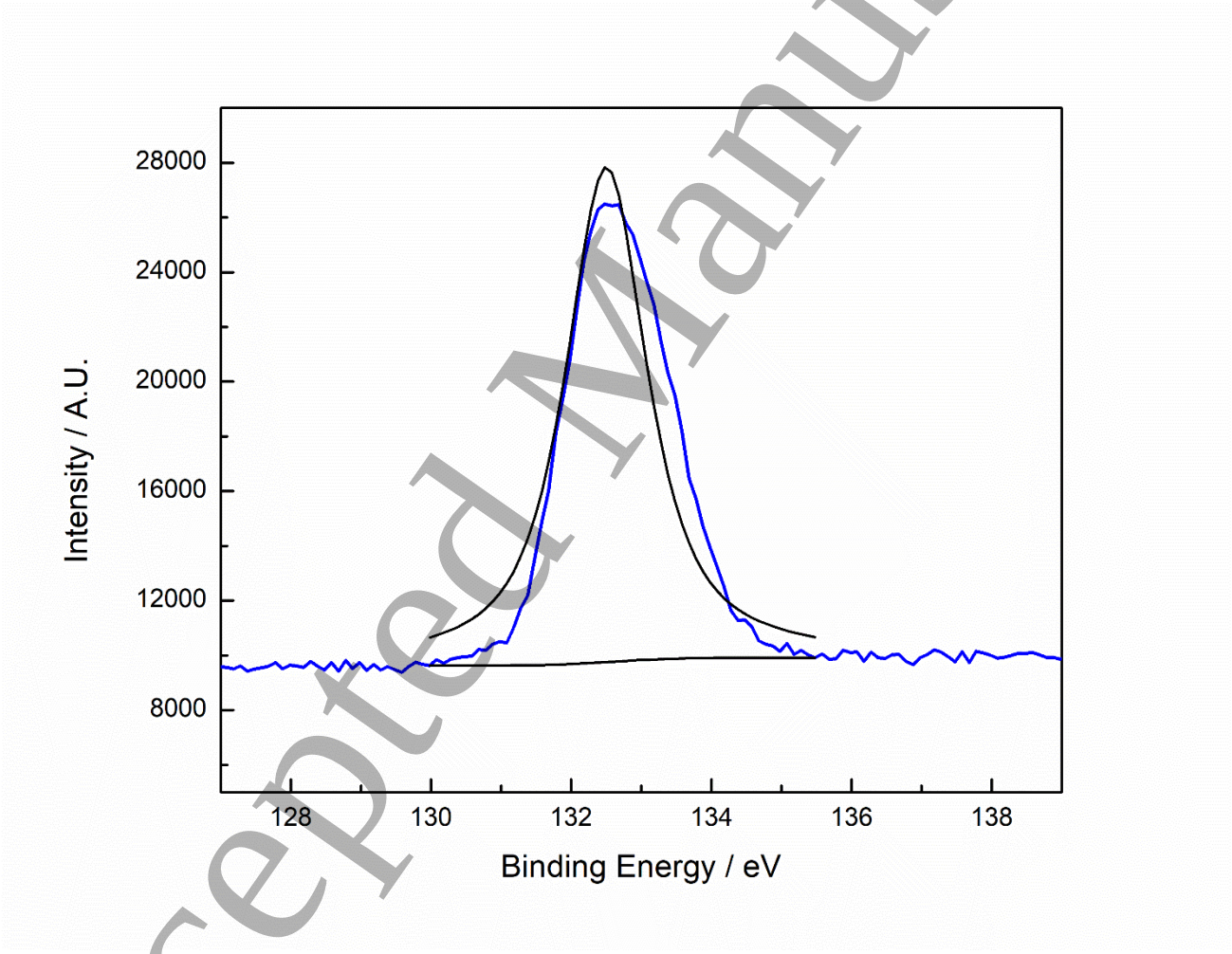

Figure 11. P2p XPS spectrum for passive layers grown on steel for 192 h at OCP in HCS+I/Cl-1. Survey spectra between 0 and 1100 eV binding energy (B.E.) were recorded with 0.1 eV steps and a bandpass of 50 eV.

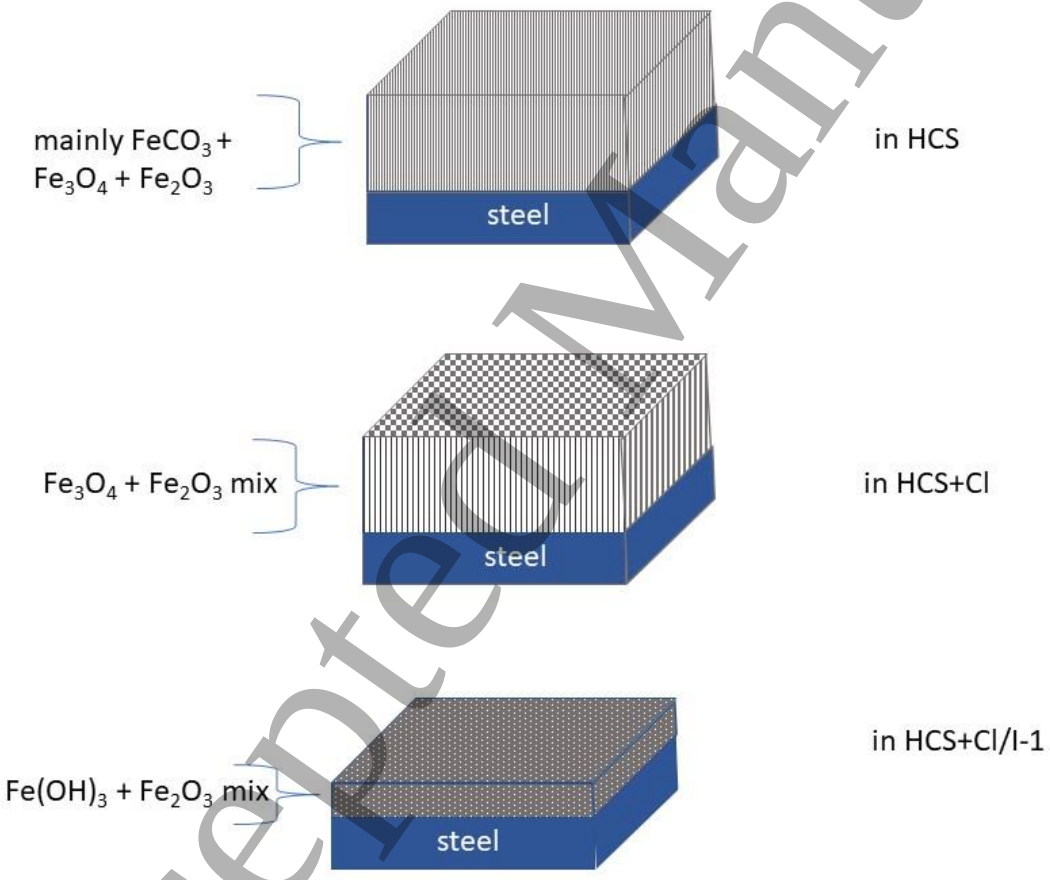

Figure 12. Differences between the surface layer comparing the three electrolytes under investigation

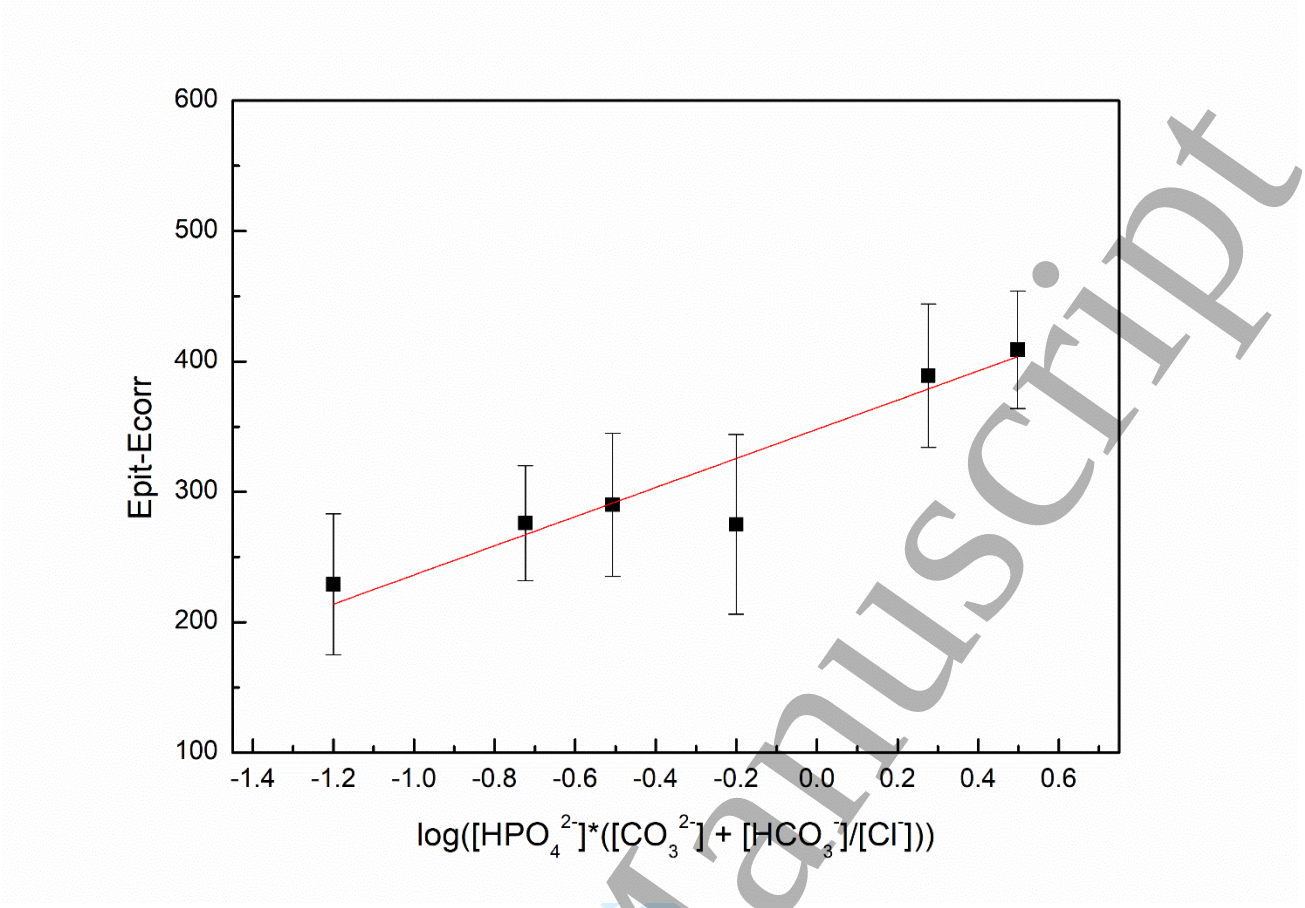

Figure 13. Logarithmic relationship between the pitting potential (*Epit* -OCP) and $\log([HPO_4^{2-}]\cdot([CO_3^{2-}] + [HCO_3^{-}]/[Cl^{-}]))$. The intercept is 348.1 mV, the slope 111.8 mV, and the regression coefficient is 0.91.

Table 1. Peaks' position and relevant associated species, relative to Figure 2a.

Peak	Position / V_{MOE}	Species
Ia	-0.63	Fe(II) oxides, hydroxides and carbonates
IIa	-0.44	Fe(II) and Fe(III) oxides and hydroxides
IIIa	-0.24	Fe(III) oxides and hydroxides
Ic	-0.48	Fe(III) compounds being reduced
IIc	-0.58	Fe(II) compounds being reduced

Table 2. Optimized parameters fitting data in Figure 3 to the equivalent circuit proposed in Figure 2, calculated from at least five independent spectra.

	HCS+Cl	HCS+I/Cl-02	HCS+I/Cl-06	HCS+I/Cl-1
OCP/mV$_{MOE}$	-235 ± 13	-193 ± 40	-169 ± 38	-152 ± 37
R_s/Ω cm^2	9.6	10.2	8.7	6.1
$ZCPE_o$/μΩ^{-1} cm^{-2}s^n	90.7	156	73.8	68.6
n_o	0.89	0.87	0.91	0.92
R_o/kΩ cm^2	5.4	1.16	14.7	56.3
$ZCPE_t$/μΩ^{-1} cm^{-2} s^n	62.2	150	21.1	8.9
n_t	0.55	0.62	0.63	0.74
R_t/kΩ cm^2	65.3	35.8	580	840

Table 3. Relevant electrochemical parameters: (a) calculated from the anodic polarization curves shown in Figure 4 and OCP values measured after 24 h at open circuit potential; (b) in a solution with 10-times less carbonate and bicarbonate content, more details in [22].

	OCP/mV$_{MOE}$	Epit/mV$_{MOE}$	Epit-OCP/mV$_{MOE}$	i pas/μA cm^{-2}
HCS$^{(a)}$	-228 ± 42	----------	----------	1.69 ± 1.31
HCS+Cl$^{(a)}$	-235 ± 13	-10 ± 13	224 ± 15	2.17 ± 1.29
HCS+I/Cl-02$^{(a)}$	-193 ± 40	155 ± 16	274 ± 69	0.31 ± 0.23
HCS+I/Cl-06$^{(a)}$	-169 ± 38	248 ± 42	389 ± 55	0.40 ± 0.14
HCS+I/Cl-1$^{(a)}$	-152 ± 37	295 ± 62	409 ± 45	0.27 ± 0.27
LCS+I/Cl-02$^{(b)}$			229 ± 54	
LCS+I/Cl-06$^{(b)}$			276 ± 44	
LCS+I/Cl-1$^{(b)}$			290 ± 55	

Table 4: Typical position of the main bands for iron and phosphate compounds

Compound	Position of the main bands (cm^{-1})
α-FeOOH	220
	280
α-Fe_2O_3	391
	484
	595
γ-FeOOH	245
	380
	1303
δ-FeOOH	485
amorphous Fe(III) oxo-hydroxides	600-800
Fe_3O_4	680
CO_3^{2-}	1080
PO_4^{3-}	940
	1005
	1081
HPO_4^{2-}	850
	989
	1080

Table 5. Weight loss results for coupons immersed in the different solutions during 42 days at OCP

	weight loss (W) /mg	description of the attack	% I	i corr /mA cm^{-2}
HCS	0.1	None	--	0.016
HCS+Cl	136.9	Pitting	---	22.1
HCS+I/Cl-1	0.2	None	99.8	0.032
HCS+I/Cl-06	0.3	None	99.7	0.048
HCS+I/Cl-02	18.9	Pitting	86.2	3.0

Table 6. Characteristic parameters associated to the elements present on the surface film.

Condition	Peak	Compounds	Binding Energy/eV	FWHM/eV	Atomic %
HCS	Fe2p	Fe^0	706.7	--	**0**
		Fe(II)	709.6	3.0	**84.6**
		Fe(III)	711	2.5	**15.4**
	O1s	O^{-2}	530	3.0	**41.3**
		OH^-	531	2.1	**1.8**
		CO_3^{2-}	532.9	2.6	**56.9**
HCS+Cl	Fe2p	Fe^0	706.7	--	**0**
		Fe(II)	709.6	2.7	**44**
		Fe(III)	711	2.7	**56**
	O1s	O^{-2}	530	2.8	**100**
		OH^-	531	--	**0**
		CO_3^{2-}	532.9	--	**0**
HCS+I/Cl-1	Fe2p	Fe^0	706.7	1.5	**8.7**
		Fe(II)	709.6	2.5	**23.7**
		Fe(III)	711	3.0	**67.6**
	O1s	O^{-2}	530	1.1	**27.8**
		OH^-	531	1.3	**63.5**
		HPO_4^{2-}	532	1.0	**8.7**
	P1s	HPO_4^{2-}	132.5	1.4	**100**